

Janus Structured Multiwalled Carbon Nanotube Forests for Simple Asymmetric Surface Functionalization and Patterning at the Nanoscale

Dr Jonathan Quinson,^{1,2,a,*} Dr Frank Dillon,¹ Dr Rebecca Nicholls,¹ Dr Antal Koos,^{1,b} Prof Kylie Vincent,² and Prof Nicole Grobert^{1,3}

¹ Department of Materials, University of Oxford, Parks Road, OX1 3PH Oxford, UK

² Department of Chemistry, University of Oxford, Inorganic Chemistry Laboratory, South Parks Road, OX1 3QR, Oxford, UK

³ Williams Advanced Engineering, Grove, Oxfordshire, OX12 0DQ, UK

Present address

^a Department of Chemistry, 5 Universitetsparken, 2100, Copenhagen, Denmark

^b Dr Antal Koos, Institute for Technical Physics and Materials Science, Centre for Energy Research, Budapest PO Box 49, Hungary

1. ABSTRACT

The asymmetric functionalization of nanomaterials is desired to develop nanostructures with increasingly exotic properties. Nevertheless, it remains a general challenge and a difficult task. Janus structured multiwalled carbon nanotubes with intra-tubular junctions between undoped and nitrogen-doped sections were exclusively considered to date for electronic applications in studies typically requiring only few individual nanotubes. Such structures are here shown to be suitable scaffolds to simply achieve a spontaneous, asymmetric and localized functionalization and patterning at the nanoscale. First, a method to produce large quantities (> 100 mg per experiment) and long (> 100 μm) vertically aligned multiwalled carbon nanotubes forests by a hybrid aerosol assisted and traditional chemical vapor deposition is presented. Scanning and transmission electron microscopy, electron energy loss spectroscopy and Raman spectroscopy characterizations confirm a continuous intra-tubular transition between nitrogen-doped and undoped sections. Second, and for the first time, the described Janus structures are shown to be suitable scaffolds to achieve an asymmetric, spontaneous and yet spatially controlled reactivity along nanotubes. This is illustrated with the examples of asymmetric oxidation properties and asymmetric immobilization of platinum nanoparticles. Asymmetric functionalization is simply achieved by carefully controlling and exploiting the different surface properties along the Janus structured carbon nanotubes.

KEYWORDS

Janus structures, carbon nanotubes, heterojunction, multiwalled, asymmetry, nanopatterning

2. INTRODUCTION

Janus nanomaterials can be defined as structures with asymmetric properties.^[1] A block copolymer or a nanoparticle with two distinct parts, e.g. two halves with different compositions, are examples of Janus structures.^[2] Such structures are typically not easily obtained and require specific techniques and/or careful design.^[1, 3] However they are yet promising objects to develop and investigate due to their unusual properties. Carbon nanotubes (CNTs) are elongated tubular and hollow nanomaterials.^[4] They are popular materials in a wide range of application and in particular conveniently used as supports for a range of molecules, particles or enzymes.^[5-7] Due to their appealing geometry, they have been considered to develop Janus-like structures.^[8] However this has exclusively been achieved by using masks, templates or local modification techniques.^[9-14] These approaches add several steps and complexity to the asymmetric functionalization of the nanomaterials. Due to the strong structures-properties relationship at the nanoscale,^[15] it is here hypothesized that asymmetric structures functionalization of CNTs can be achieved *spontaneously*, without using local modification techniques, by precisely controlling in the first place the surface properties of CNTs during their synthesis. Developing such scaffolds is indeed yet to be applied for simple patterning at the nanoscale.

Interestingly, CNTs with intra-tubular junctions have been reported.^[16, 17] These consist of nanotubes with different sections showing different compositions. They are typically obtained by changing the nature of the precursor used during the synthesis of the different sections. A typical example is CNTs with a junction between an undoped section and a nitrogen-doped section. Nitrogen-doping results in a strong change in the CNT structural and surface properties.^[18-20] A first challenge in the synthesis of CNT with intra-tubular junctions is to develop a continuous interface between the different sections. To date, these structures have been exclusively studied

for their p-n junction properties.^[21, 22] The limitation of their scope of application to electronics can be inferred to the limited quantity of materials prepared (previous studies typically required only a few individual CNTs) and the limited length achieved (typically 10s of micrometers) for CNTs with junction.^[16, 22, 23]

Here, a method to produce several milligrams and multiwalled CNT (MWCNTs) longer than 100 μm with intra-tubular junctions between nitrogen-doped and undoped sections is first reported. Second, the Janus structured MWCNT ‘forests’ scaffolds obtained *via* this method are shown for the first time to have asymmetric properties *along* the tubes. This is illustrated with the example of asymmetric oxidation properties and the MWCNTs are further applied as scaffolds to achieve a simple, asymmetric, spontaneous and yet spatially controlled immobilization of platinum nanoparticles along the MWCNT outer surface.

3. EXPERIMENTAL SECTION

Chemicals. $\text{C}_6\text{H}_5\text{CH}_2\text{NH}_2$ ($\geq 99\%$, Fluka), $\text{C}_6\text{H}_5\text{CH}_3$ (99.9 %, Fluka), KH_2PO_4 ($\geq 99\%$, Sigma), K_2HPO_4 ($\geq 98\%$, Sigma-Aldrich), $\text{H}_2\text{PtCl}_6 \cdot 6\text{H}_2\text{O}$ (ACS reagent, Sigma-Aldrich), H_2SO_4 (98%, Fisher Scientific), HCOOH (98%, Fluka), KCl (99.5%, Fisher Scientific) were all used as received. $\text{C}_{10}\text{H}_{10}\text{Fe}$ (98 %, Aldrich) was purified by sublimation at 90 $^\circ\text{C}$ prior to use. Argon (99.99%), hydrogen (99.995%), ammonia ($\geq 99.98\%$), acetylene (industrial grade) were obtained from BOC. Millipore MilliQ (18 $\text{M}\Omega\text{ cm}$) water was used for platinum electrochemical or chemical reduction.

MWCNT forest synthesis. Nanotube forests were synthesized using both liquid-liquid and liquid-gas precursors following a general approach illustrated in **Scheme 1**.

(a). Liquid-liquid (liq-liq) synthesis, illustrated in **Figure S1**. Vertically aligned MWCNTs were grown on silicon wafer substrates (10 x 20 mm², Sibert, UK) using an aerosol assisted chemical vapor deposition setup consisting of a piezoelectric generator, a quartz tube (2.2 cm inner diameter), a 50 cm long horizontal tube furnace, gas flow controllers and an acetone gas trap.^[18-20] A solution of 5 wt.% ferrocene (the iron catalyst precursor) in toluene (the carbon source) was used for the synthesis of an undoped section. A solution of 5 wt.% ferrocene (the iron catalyst precursor) in benzylamine (the nitrogen and carbon source) was used for the synthesis of a N-doped section. To induce an intra-tubular junction, the hydrocarbon precursor sources were switched during a same synthesis. This was accomplished by having a separate aerosol unit connected to the main setup but closed off until required. The synthesis temperature was 800 °C with Ar as carrier gas at a flow rate of 2500 sccm (standard cubic centimeters per minute) for all experiments. By varying the length of time one precursor was introduced in comparison to the other, it is possible to grow undoped sections longer than N-doped sections or *vice versa*.

(b) Liquid-gas (liq-gas) synthesis, illustrated in **Figure S2**. A combination of liquid and gas precursors was used. Liquid precursors containing ferrocene 5 wt.% were: toluene for C and benzylamine for N sections of MWCNTs; gas precursors were: acetylene for C and ammonia together with acetylene for N sections. Argon was used as a carrier gas for liquid precursors and hydrogen together with argon for gas precursors. The total flow was 2500 sccm in all cases and experiments were performed at 800 °C. Typically argon/hydrogen/acetylene flow rates in sccm were: 2000/400/100 and argon/hydrogen/acetylene/ammonia flow rates in sccm were: 2000/400/50/50. By varying the length of time one precursor was introduced in comparison to the other, it is possible to grow undoped sections longer than N-doped sections or *vice versa*.

Platinum nanoparticle deposition. Platinum particles were electrodeposited using a three-electrodes setup. The working electrode was a MWCNT forest as-prepared on a silicon wafer, the reference electrode a standard calomel electrode (SCE), the counter electrode was platinum. Measurements were performed with an Autolab128N potentiostat (EcoChemie, Netherlands) controlled by GPES software. Pre-treatment consists in scanning 10 times the samples at a 50 mV s⁻¹ scan rate in H₂SO₄ (0.1 M) between -0.3 and 1.3 V vs SCE (BAS). Platinum electrodeposition was performed with a solution of H₂PtCl₆.6H₂O (5 mM) in potassium phosphate buffer (50 mM, pH=7) or KCl (50 mM) electrolyte by cycling 3 to 30 times the potential between -0.75 and 0.25 V vs SCE at a scan rate of 50 mV s⁻¹. Alternatively, platinum deposition was performed by chemical reduction at room temperature and in air by dropping the MWCNT forests on silicon wafers into a solution of H₂PtCl₆.6H₂O (1.5 mM) prepared in a mixture of H₂O:HCOOH (20:1, v:v). Samples were left into the solution for 3 to 8 hours.^[24-26] Samples were subsequently thoroughly washed with water and dried in air at room temperature.

Characterization. The MWCNTs were characterized using a SEM Jeol 840F operated at 5 kV equipped with a secondary electron detector and a Zeiss NVision FIB microscope equipped with an in-lens and a backscattered electrons detector also operated at 5 kV. For clarity, cross section images were obtained after cleaving the silicon wafer so as to expose the inside of the MWCNT forests. A simple mechanical pressure on the edge of the silicon wafer used as substrate was enough to achieve the section.

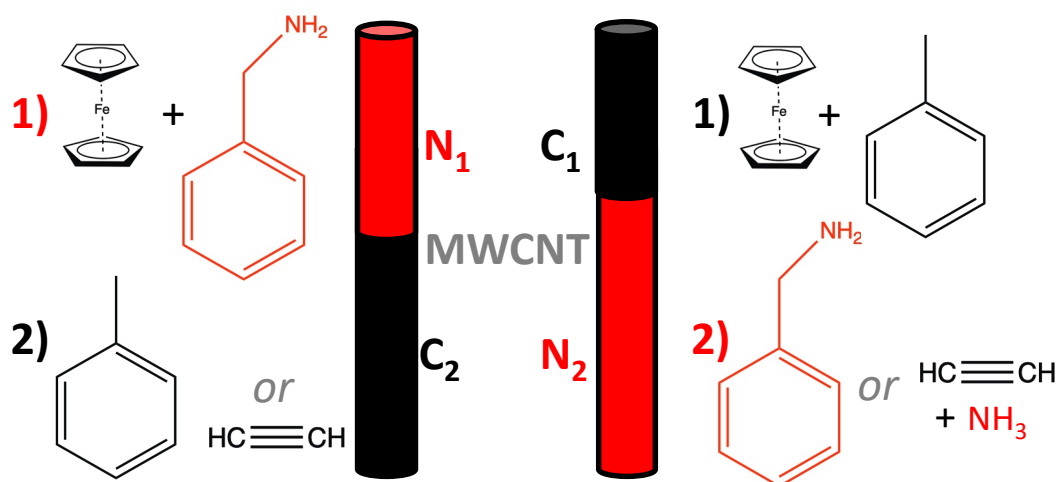
TEM images were taken with a Jeol 2000FX operated at 200 kV. STEM-EELS measurements were performed at the University of Warwick with a Jeol ARM200F operated in STEM-ADF mode at 80 kV to reduce knock-on damage caused by the beam.^[27] The degree of graphitization of the samples was investigated using a JY Horiba Labram Aramis imaging confocal Raman microscope with a 532 nm excitation. TGA measurements were performed with a Perkin Elmer

Pyris Thermogravimetric Analyser from 100 °C to 900 °C at 5 °C min⁻¹. EDS mapping and associated SEM backscattered images were recorded with a Hitachi TM3000 table top SEM operated at 15 kV. For Pt and Fe mapping the 2.100 keV and 6.399 keV peak intensities were used.

4. RESULTS AND DISCUSSION

4.1. Janus structured MWCNT forests: liquid-liquid synthesis approach

A natural approach to tune the properties *along* a CNT is to change the properties of precursors used *during* the synthesis.^[28, 29] Different approaches were explored using an aerosol assisted chemical vapor deposition synthesis detailed in the experimental section. A key idea is to switch the nature of the precursor as illustrated in **Scheme 1**. In a first approach referred to as liquid-liquid (liq-liq), the precursors used to grow the first (1) and the second (2) sections of the MWCNTs with intra-tubular junctions are both liquid precursors. These precursors were previously studied independently:^[6, 18, 20] toluene was used to grow undoped section referred to as ‘C’, whereas benzylamine was used to grow a nitrogen-doped section referred to as ‘N’ typically characterized by graphitic as well as pyridinic and pyrrolic molecular nitrogen in the carbon structure with up to 2.2 at.%.^[18, 20, 30] A carbon nanotube is never a ‘pure’ carbon material since chemical elements like oxygen are typically present. The term *undoped* in the context of this study must be understood as *undoped on purpose* or *with no design to promote a significant doping*.



Scheme 1. Schematic representation of the synthesis and precursors used to develop MWCNTs with N_1/C_2 and C_1/N_2 structures from different liquid or gas precursors.

Scanning electron microscopy (SEM) micrographs of $C_{1\text{-liq}}/N_{2\text{-liq}}$ and $N_{1\text{-liq}}/C_{2\text{-liq}}$ structures are shown in **Figure 1a** and **Figure 1b**, respectively (the sequence of N or C precursor injection is indexed in numerical order in text and Figures, see experimental section for more details and **Figure S3** in Supplementary Information for further SEM micrographs). The typical structure of vertically aligned MWCNT ‘forests’ or ‘carpets’ is observed.^[4] For both samples, a morphological change is observed along the tubes: one section of the nanotube forest is much straighter than the other wavier section. N-doped MWCNTs are known to be straighter than undoped MWCNTs.^[6, 18-20] The sections are here long enough to be unambiguously identified using a simple optical microscope, see **Figure S4**. This makes it possible to acquire unambiguously Raman spectra along the MWCNT forests as displayed in **Figure 1e-f**. A MWCNT spectrum is characterized by so called D, G and 2D peaks around 1340, 1565 and 2680 cm^{-1} , respectively, see also **Figure S4**. The straight sections show an intensity ratio between the D and G peak (I_D/I_G) value about 1 and a nearly non-existent 2D peak. On the more wavy sections, the MWCNTs show a I_D/I_G value less

than 1 and a marked 2D peak. These are exactly the signals expected from N-MWCNTs and undoped MWCNTs, respectively.^[6, 18-20] This confirms points towards the evidence that the wavy sections are made of undoped MWCNTs whereas the straighter sections are N-doped. Knowing the sequence of synthesis performed, the attribution of the different sections confirms in a very simple way (e.g. compared to previous studies using carbon isotopes^[31, 32]) that the MWCNTs grow by a root-growth mechanism,^[33] see **Figure S5**.

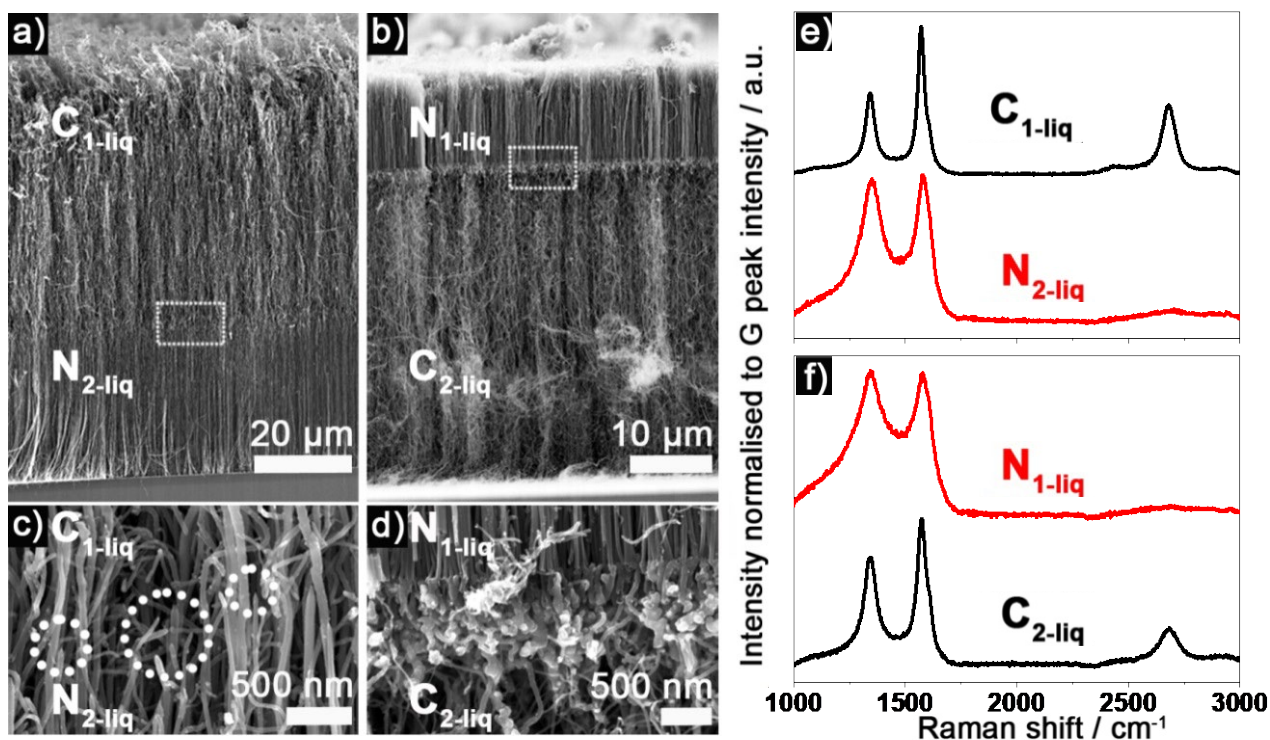


Figure 1. SEM micrographs of (a) C_{1-liq}/N_{2-liq} and (b) N_{1-liq}/C_{2-liq} MWCNT forests on silicon wafers (at the bottom of the micrographs). Such structures are obtained whether or not ferrocene catalyst precursor is present in the second precursor. Higher resolution micrographs of the interface between N and C sections identified by the square box in (a) and (b) are displayed in (c) and (d) respectively. Broken MWCNTs are observed at the C₁/N₂ interface and are highlighted in dotted circles in (c). Raman spectra of each section for each structure are reported in (e) for a C_{1-liq}/N_{2-liq} and (f) for a N_{1-liq}/C_{2-liq}.

Higher magnification SEM micrographs show that the junctions formed between the two sections are not continuous. Broken MWCNTs are present at a C₁/N₂ interface, dotted circles in **Figure 1c**, and a strong morphological change without continuity in the tube structure is observed at a N₁/C₂ interface, **Figure 1d**. The reasons for this discontinuity may originate from a flow perturbation during the relatively poorly controlled switch of the precursors in the liquid-liquid approach. In addition, N-doped MWCNTs and undoped MWCNTs have different inner diameters. Undoped MWCNTs have typically a smaller inner diameter than N-MWCNTs,^[6, 20, 22] see also **Figure S5** for illustration. It is expected that the size of the iron particles needed to catalyze the growth of the N section are then larger than to grow the C section.^[4] Additionally, nitrogen acts as a “poison” for iron catalysts in CNT growth,^[34, 35] likely causing a pause in the growth of the CNT when nitrogen is introduced and thus causing a break in the tube structure. The detailed changes occurring on the catalyst as the MWCNTs grow under different conditions certainly shape the property of the resulting nanomaterial in a complex interplay between catalyst properties, carbon feedstock and other reactions conditions like temperature and presence of nitrogen.^[36-39]

From this first liquid-liquid approach, a significant achievement is to produce long (> 100 µm) Janus structured MWCNT forests with different sections in relatively high yield (> 100 mg per experiment) by simply switching the nature of the precursor used to grow each section. However, achieving a continuous interface remains a challenging task.

4.2. Liquid-gas synthesis approach

In order to develop a continuous junction between the different sections, a different synthesis approach referred to as liquid-gas (liq-gas) was developed also illustrated in **Scheme 1**. It involves using liquid precursors *via* aerosol assisted chemical vapor deposition and gas precursors *via* chemical vapor deposition. The gases used to grow the C section were acetylene whereas acetylene together with ammonia were used for the N section. SEM micrographs of the nanomaterials obtained using the liquid-gas approach are displayed in **Figures 2 and 3**. MWCNTs with lengths over 100 μm are easily formed and a morphological, **Figure 2a-b**, and structural, **Figure 2e-f**, change is observed between the two sections, especially in the case of structures with N_1/C_2 junctions. Here as well, in analogy with the liquid-liquid approach detailed above and in agreement with results obtained studying the different sections synthesized separately,^[6, 18] the N sections are straighter than the C section and the N section have an I_D/I_G value about 1 and a less marked 2D peak. The C sections have a I_D/I_G value less than 1 and a marked 2D peak. However, unlike the liquid-liquid approach, both junctions (N_1/C_2 and C_1/N_2) are now continuous, **Figure 3a-b**: the SEM micrographs do not display broken MWCNTs or the presence of particle-like structures that break the continuity of the MWCNTs. The $\text{N}_{1\text{-liq}}/\text{C}_{2\text{-gas}}$ interface is marked by presence of a lighter line in the SEM micrographs. Energy X-ray spectroscopy (EDS) analysis at this position confirms that the $\text{N}_{1\text{-liq}}/\text{C}_{2\text{-gas}}$ interface is mainly made of iron from the catalyst particles, **Figure S6**. The presence of these nanoparticles at the N_1/C_2 junction is discussed in more details later. The major improvement brought by the liquid-gas approach is the formation of a continuous interface between the different sections.

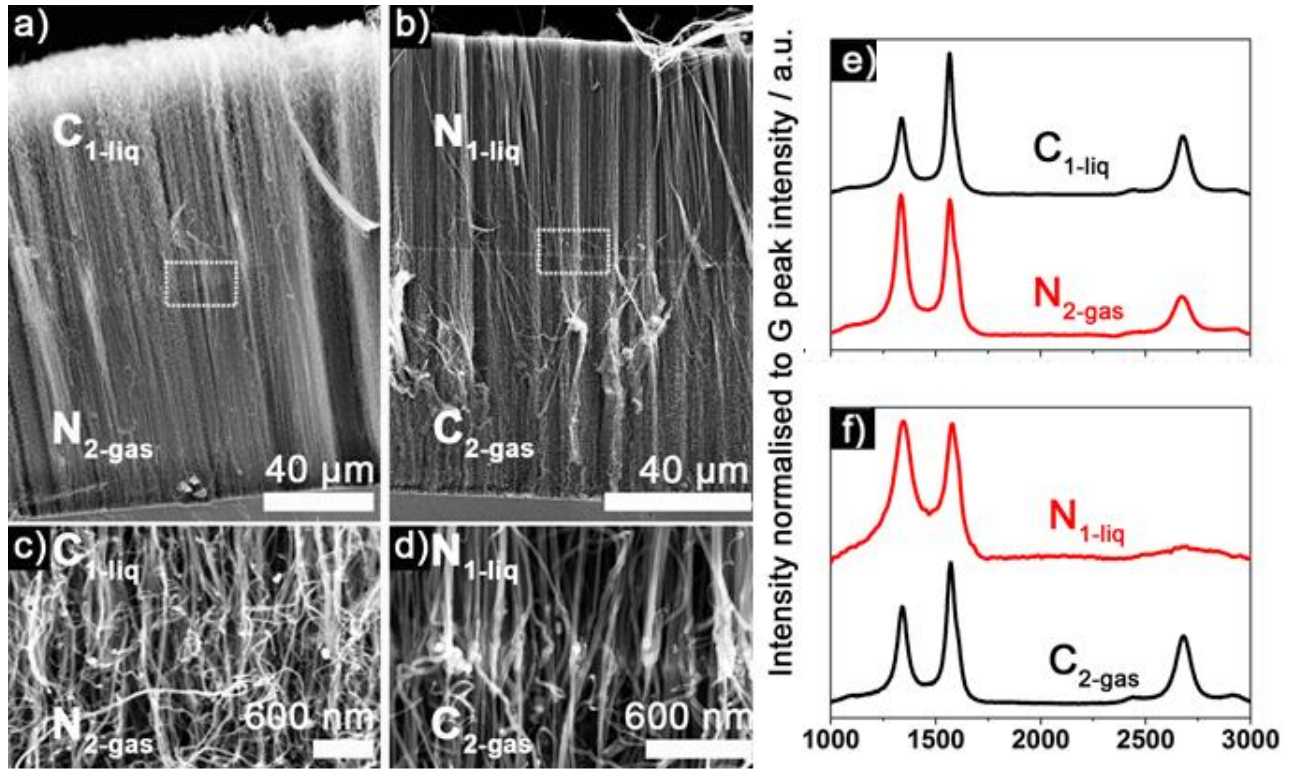


Figure 2. SEM micrographs of (a) $C_{1\text{-liq}}/N_{2\text{-gas}}$ and (b) $N_{1\text{-liq}}/C_{2\text{-gas}}$ vertically aligned MWCNT forests. Higher resolution images obtained for the interface between N and C sections identified by the square box in (a) and (b) are displayed in (c) and (d) respectively and suggest continuous interfaces in a liquid-gas approach. Raman spectra of each section for each structure are reported in (e) for a $C_{1\text{-liq}}/N_{2\text{-gas}}$ and (f) for a $N_{1\text{-liq}}/C_{2\text{-gas}}$.

4.3. Detailed characterization of a MWCNT intra-tubular junction

Transmission electron microscopy (TEM), scanning TEM (STEM) micrographs and energy electron loss spectroscopy (EELS) measurements performed at the interface on a $N_{1\text{-liq}}/C_{2\text{-gas}}$ sample are shown in **Figure 3c-f**. The presence of catalyst particles at the N_1/C_2 interface^[28] is here conveniently used as an interface marker for further characterization: elongated darker features in TEM micrographs, elongated whiter features in SEM and STEM micrographs. On one side of the

interface (marked by presence of iron based particles), the typical structure of N-MWCNTs is observed: a corrugated structures with a larger inner diameter. On the other side of the interface, the typical structure of an undoped MWCNT is identified:^[6, 20] smaller inner diameter (lighter inner part of the tube) and thicker walls (darker part of the tube), **Figure 3c**. Moreover, on the corrugated side of the interface, gaseous nitrogen was detected using EELS as assessed by presence of N-K edge peak detailed in the inset of **Figure 3e**, whereas no nitrogen was detected from the non-corrugated section. This confirms that within 100 nm of the interface marked by a nanoparticle, a complete change in structure, and hence functionality and chemistry, can be induced by a change in precursor during synthesis.

The ability to mark the interface by the presence of catalyst particles makes the identification of the interface easy and reliable on TEM grids. It can be suggested that the driving force for a nanoparticle to be located at a N_1/C_2 interface is a need for a change in nanoparticle size. The nanoparticle catalysts formed here from ferrocene are located at the root of the nanotube, in direct contact with the substrate and in agreement with a root growth mechanism, see **Figure S5, S7**. A N_1/C_2 interface requires a size decrease which can be achieved by ‘losing’ some of the catalyst within the tube (undoped MWCNTs have a smaller diameter than N-MWCNT and so are grown from smaller nanoparticles^[4]). A C_1/N_2 interface requires a size increase, probably simpler to achieve by merging of smaller nanoparticles present on the substrate, which explains the absence of nanoparticles at a C_1/N_2 interface. These results also support the fact that using a gas precursor in the second step of the growth improves the formation of continuous N_1/C_2 and C_1/N_2 interfaces. Interestingly, it is shown that the catalyst nanoparticles formed from ferrocene during the growth of the liquid precursor remain active long enough to support the growth from another precursor, liquid or gas, see **Figure S4, S7**.

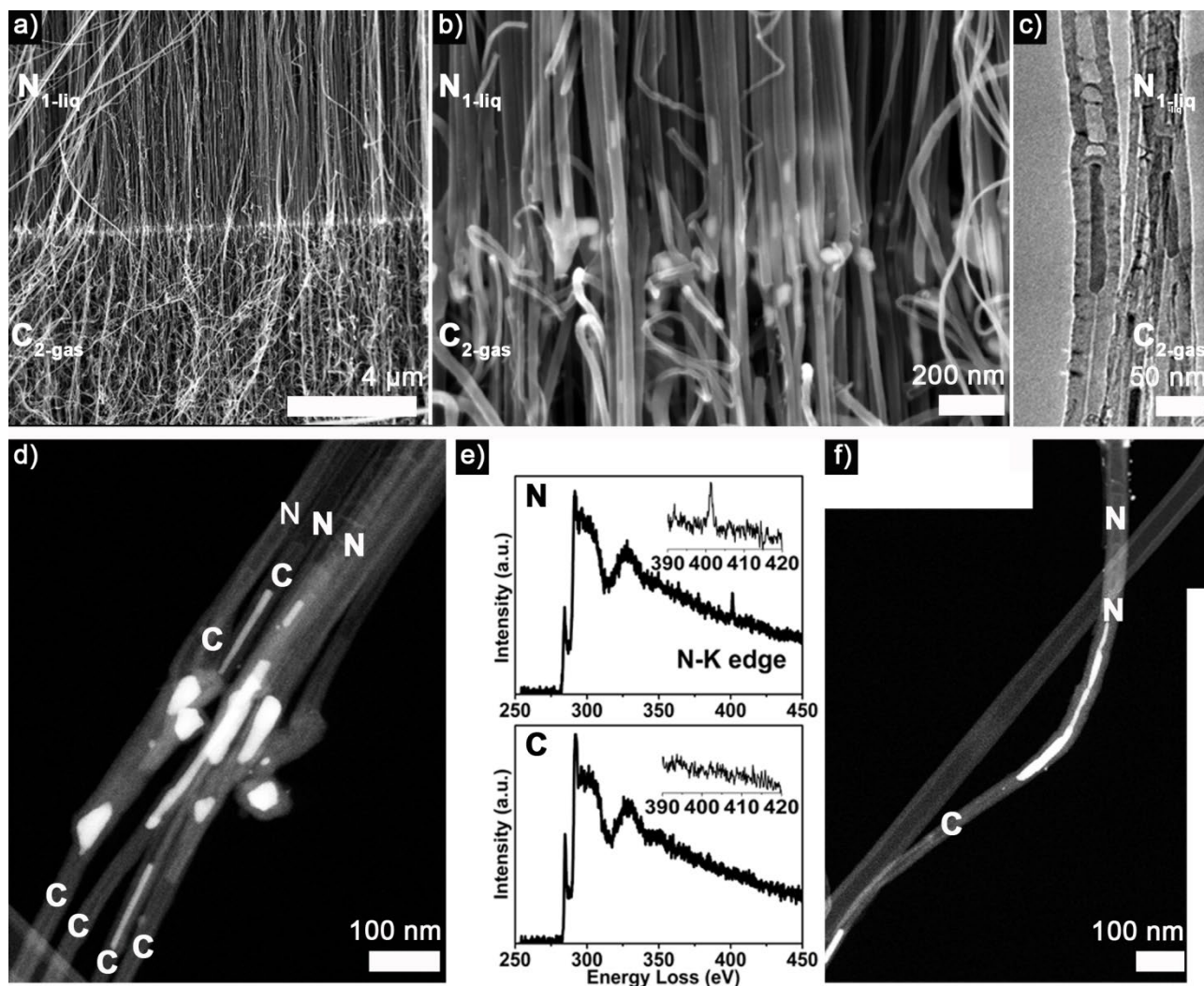


Figure 3. (a) and (b) SEM micrographs of N₁-liq/C₂-gas MWCNT structures at different magnification. The presence of catalyst particles marks the interface. (c) TEM micrographs, of the previous interface, reconstructed from 3 TEM micrographs taken at the same magnification. (d) and (f) STEM micrographs of N₁-liq/C₂-gas MWCNT structures. Presence of catalyst particles, in white on the STEM dark field images, acts as a marker of the interface. Letters C or N on the STEM images (d) and (f) spot parts of tubes where EELS signal expected for respectively undoped MWCNTs and N-MWCNTs where observed. The associated EELS signals are reported in (e).

4.4. Asymmetric oxidation properties

To demonstrate for the first time the difference in properties between each of the sections in the Janus structures, thermogravimetric analysis (TGA) characterization was performed on samples created *via* the liquid-gas approach, **Figure 4a**. TGA was never reported for such structures which can be inferred to the limited yield and length in previous studies. TGA curves for MWCNTs without junctions show only one smooth curve and the oxidation resistance of MWCNT is higher than for N-MWCNTs.^[18, 20] Here, two distinct parts in the oxidation curves are observed, separated by an inflection at *ca.* 550-555 °C. Since the samples have both an undoped and a N-doped section, it is likely that the mass loss before the inflection (lower temperature) is related to the N section (more reactive) and the mass loss after the inflection (higher temperature) is related to the C section, in agreement with previous characterization of the different sections grown separately.^[18, 20]

To investigate further this unusual oxidation behavior for CNTs, various samples showing N₁/C₂ or C₁/N₂ junctions were oxidized in air at 520 °C: a temperature lower than the temperature of the observed inflection around 555 °C. Representative Raman spectra are shown in **Figure 4b**. In all cases the N section disappears after oxidation: the expected peaks in the Raman spectra of N-MWCNTs cannot be recorded anymore: see continuous-red line in **Figure 4b**. Conversely, the C section of the MWCNTs remains detectable using Raman spectra: see dotted line in **Figure 4b**. The carbon structure is however damaged by oxidation, as evidenced by the higher *I_D/I_G* ratio of the C section after oxidation. In addition, SEM micrographs of the Janus structures before, **Figure 4c**, and after, **Figure 4d,e**, oxidation confirm a selective oxidation of the N section. Regardless of the synthesis route, this selective reactivity of the N section compared to the C section was observed for different junctions: N₁/C₂ or C₁/N₂, **Figure S8** and C₁/N₂/C₃ in **Figure S9**.

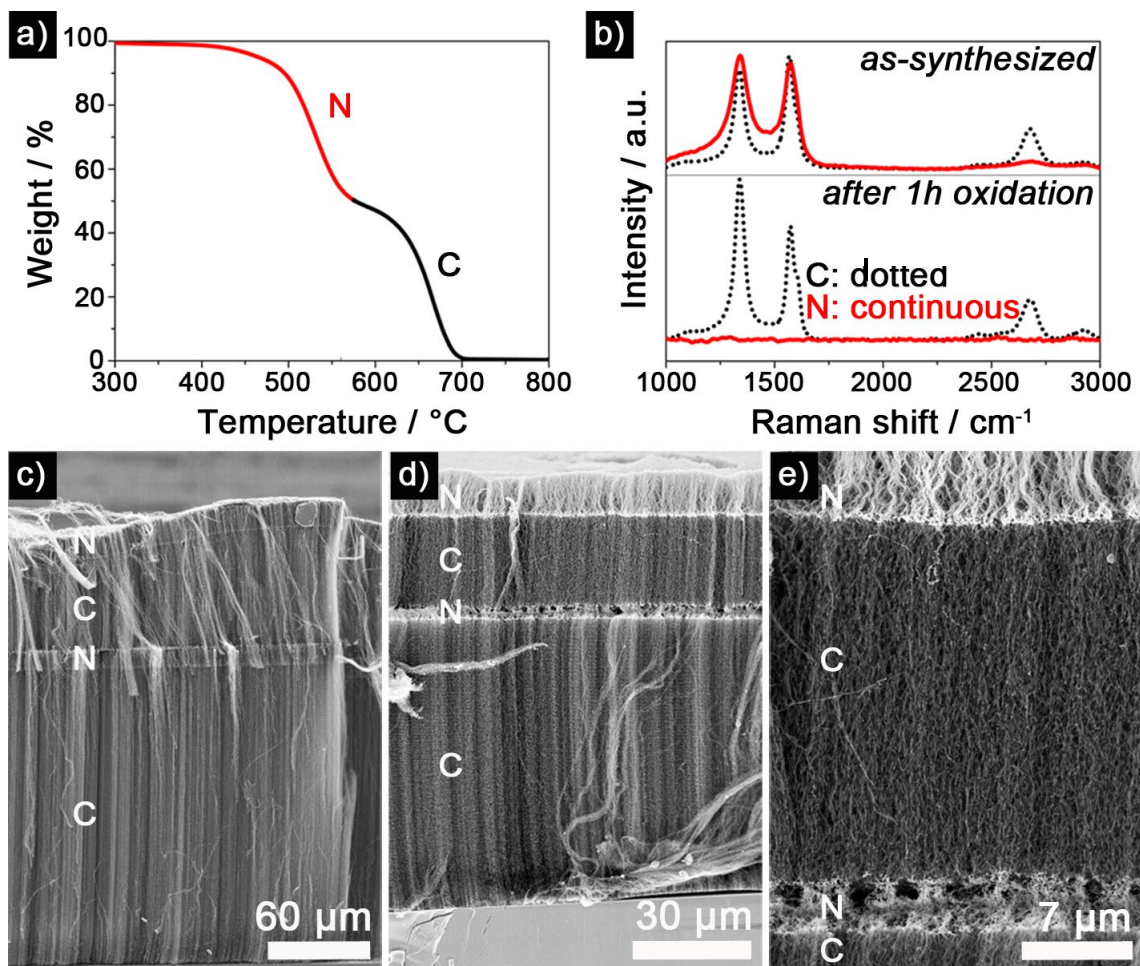


Figure 4. (a) TGA curve for a N₁-liq/C₂-gas structure. Weight loss before the inflection point at ca. 555 °C is related to the oxidation of the N section whereas the weight loss after the inflection point is related to the C section. (b) Raman spectra of both N (continuous) and C (dotted) sections before (top) and after (bottom) oxidation in air for 1 hour at 520 °C. (c-e) SEM micrographs of N₁-liq/C₂-gas/N₃-liq/C₄-gas structure before (c) and after (d-e) oxidation in air for 30 min at 520 °C.

4.5. Asymmetric immobilization of platinum nanoparticles

Nitrogen doping induces defects in the structure of CNTs and the resulting N-CNTs are more chemically reactive than their undoped counterparts.^[18] The direct formation of platinum particles

on the N-MWCNT outer surface leads to a more homogenous coverage than for undoped MWCNTs.^[7] Several factors can explain the better dispersion of Pt nanoparticles on N-CNTs: better wettability of N-CNTs allowing better Pt particle deposition, higher density of nucleation sites in the more defective N-CNTs, different electronic properties since N-CNTs have an electron donor-like behavior favoring a more uniform nucleation and stronger Pt-N interactions.^[7, 40] The structural differences and localized oxidative behavior observed along the Janus structured MWCNT forests prepared here points towards a difference in the outer surface properties between N and C MWCNT sections. To demonstrate that forests of MWCNTs with N₁/C₂ or C₁/N₂ junctions have different functionalities *embedded* in their structures and designed *during* synthesis, platinum particles were immobilized by bulk electro-deposition of platinum salts^[41] or by bulk chemical reduction.^[42-44] In all cases, both N and C sections were dipped into the same platinum salt solution. Regardless to the approach used to nucleate the platinum particles, a difference in nanoparticle loading between the N and C sections is clearly observed. SEM micrographs in **Figure 5** show that the particles coverage differs from the C, **Figure 5b** and the N, **Figure 5c**, sections of the forest, with a more uniform coverage on the N section. This result is independent of the type of electrolyte used, the method of deposition used or the time used for deposition, see experimental section and **Figure S10**.

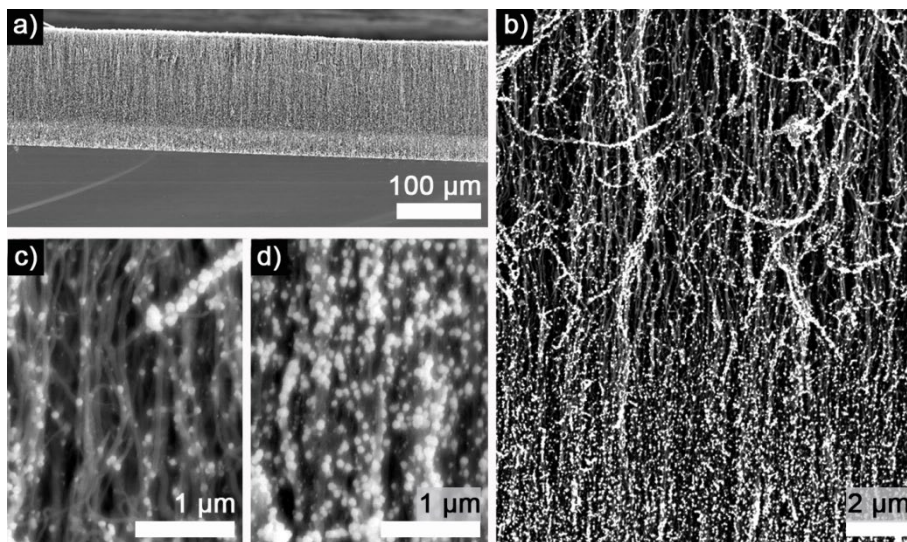


Figure 5. (a) and (b) SEM images of a C_{1-liq}/N_{2-liq} MWCNT structure after electrodeposition of platinum nanoparticles. (c) and (d) are higher magnification SEM images of the C and N sections displayed in (a) and (b) respectively. The C section is at the top of the images in (a) and (b) whereas the N section is at the bottom.

Backscattered electron SEM micrographs, **Figure 6**, also confirm the higher concentration of platinum nanoparticles on the N section of the Janus structure as the N section comes out lighter than the C section, **Figure 6a-d**. This difference is not due to the residual iron based particles in/on the CNT as this difference in contrast is not observed on control experiments where no platinum deposition was performed, **Figure 6e-f**.

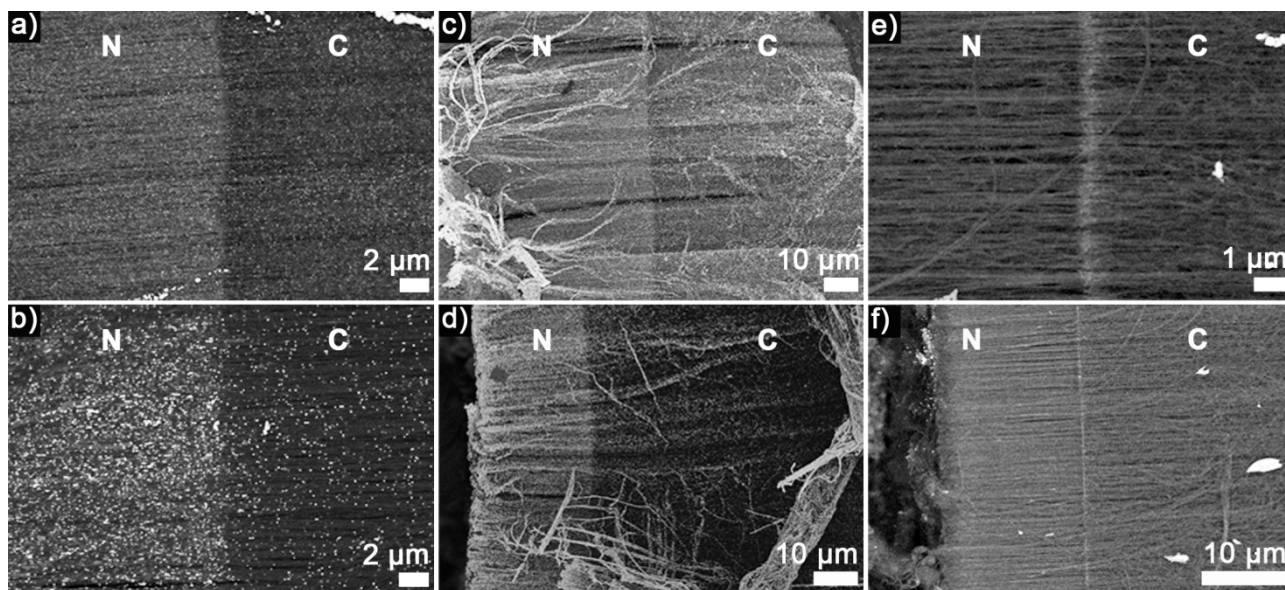


Figure 6. SEM micrographs (backscattered electron detector for two different MWCNT forests with N₁-liq/C₂-gas junctions. (a), (c) and (e) refer to a N₁(60 μm long)/C₂(70 μm long) structure and (b), (d) and (f) to N₁(20 μm long)/C₂(70 μm long) structure. (a), (b), (c) and (d) show samples after platinum bulk electrodeposition. (e) and (f) are micrographs from the samples before platinum was immobilized. The lighter line observed (e) and (f) comes from iron based particles marking the junction.

Finally, electron dispersive X-ray spectroscopy (EDS) mapping, **Figure 7**, makes it possible to confirm a more prominent platinum signal from the N section of the tubes in comparison to the C part: more uniform coverage of the green dots related to presence of platinum on the N section rather than the C section, see also **Figure S11**. Conveniently the synthesis methods presented allow producing structures with C₁/C₂, N₁/N₂ as well as C₁/N₂ and N₁/C₂ junctions, with different length for each section by changing the time of injection of the relevant precursors (see also **Figure S3**). Then same functionalization experiments performed on such control structures support that the

asymmetric functionalization observed does not result simply from different sections grown from different precursors but indeed because a C/N or N/C interface was designed.

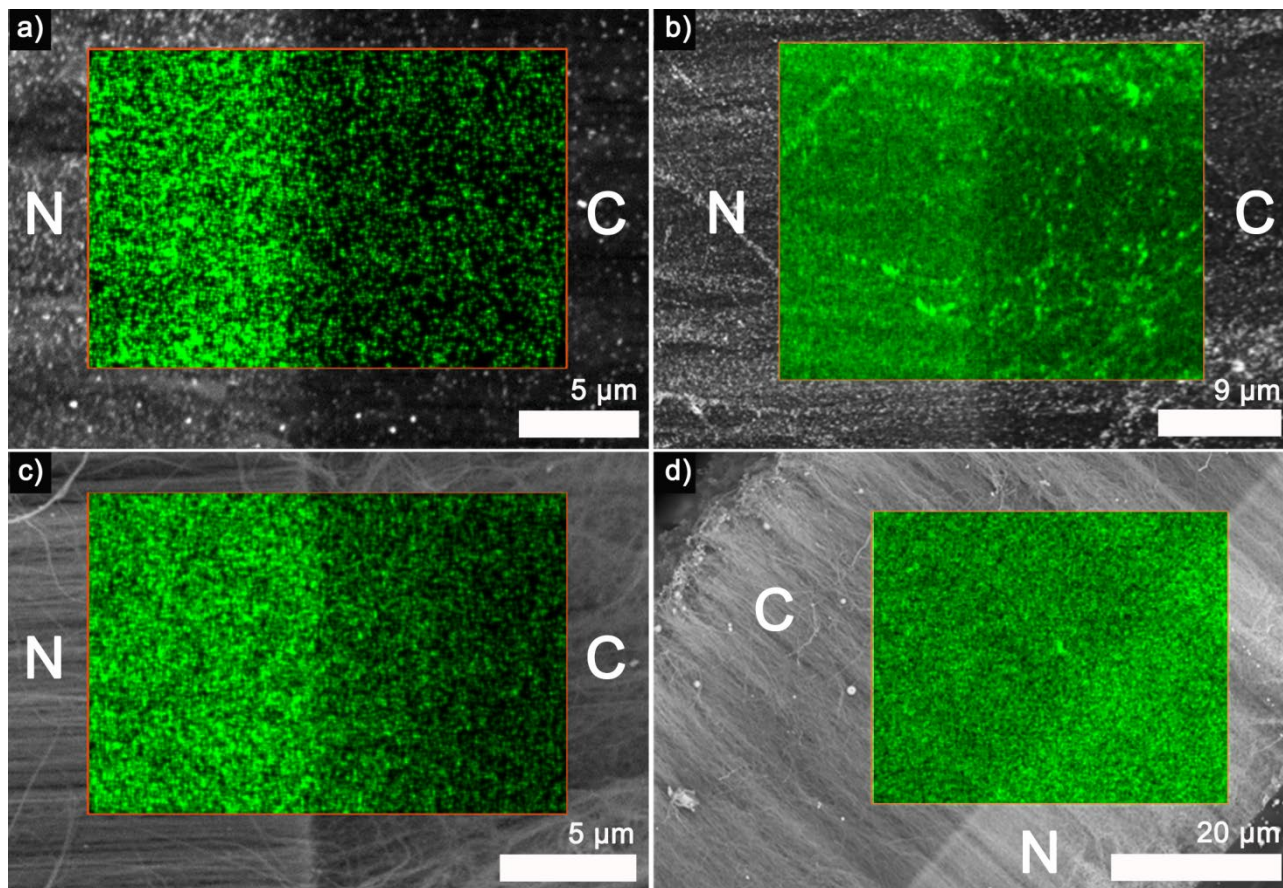


Figure 7. Backscattered electron micrographs and platinum (green) EDS maps of (a-c) $\text{N}_{1\text{-liq}}/\text{C}_{2\text{-gas}}$ and (d) $\text{C}_{1\text{-liq}}/\text{N}_{2\text{-gas}}$ structures on which platinum was deposited whether by (a) and (b) electro-deposition or (c) and (d) chemical reduction. The difference between samples displayed in (a) and (b) is a different N/C length ratio of $\text{N}_1(20\text{ }\mu\text{m})/\text{C}_2(70\text{ }\mu\text{m})$ and $\text{N}_1(60\text{ }\mu\text{m})/\text{C}_2(70\text{ }\mu\text{m})$ respectively.

5. CONCLUSION

Janus structured multiwalled carbon nanotube forests, consisting of vertically aligned MWCNTs with high quality intra-tubular junctions between undoped and nitrogen-doped sections, were synthesized using a combination of liquid and gas precursors and characterized. Relatively large amount (> 100 mg per experiment) and long (> 100 μm) MWCNTs are obtained. This is directly relevant for their previously established applications in electronics. The different surface properties along the MWCNTs are here successfully exploited to promote asymmetric and localized oxidation properties as well as asymmetric immobilization of platinum particles on different sections of the MWCNTs. Those results demonstrate for the first time the facile creation of Janus structures *along* a CNT where a controlled asymmetric immobilization is induced by structural design rather than a post-synthesis functionalization techniques. It is shown that such design can easily be applied for simply patterning structures at the nanoscale.

The results show that beyond their electronic properties, MWCNTs with intra-tubular junctions are promising nanomaterials directly relevant to develop and apply further complex functionalized materials. Since the different sections of the MWCNT forests are easily distinguished by optical microscopy and Raman spectroscopy it is likely that optical microscopy coupled with Raman, infra-red, fluorescence spectroscopy or other techniques could prove to be facile characterization for the localized asymmetric immobilization and functionalization with of other particles, molecules or proteins on specific sections of the detailed scaffolds.

ASSOCIATED CONTENT

Supporting Information. The following files are available free of charge. SEM, Raman and EDS data, schematic representation of growth mechanism, schematic representation of experimental set-up (PDF).

AUTHOR INFORMATION

Corresponding Author

* E-mail: jonathan.quinson@chem.ku.dk

Present Addresses

† Chemistry Department, University of Copenhagen, 5 Universitetsparken, København Ø, 2100 København, Denmark

Author Contributions

The manuscript was written through contributions of all authors. All authors have given approval to the final version of the manuscript.

Funding Sources

The Engineering and Physical Sciences Research Council is thanked for an EPSRC DTA award EP/J500495/1.

ACKNOWLEDGMENT

K. A. Vincent is thanked for access to electrochemical equipment. The nanomaterial by design group, University of Oxford UK is thanked for access to equipment. R. J. Nicholls is thanked for

her help in EELS data acquisition. F. Dillon is thanked for running TGA measurements. A. Koos is thanked for fruitful discussion.

6. REFERENCES

- [1] Loget, G.; Kuhn, A., Bulk synthesis of Janus objects and asymmetric patchy particles. *J. Mater. Chem.* **2012**, *22* (31), 15457-15474.
- [2] Loget, G.; Roche, J.; Kuhn, A., True bulk synthesis of Janus objects by bipolar electrochemistry. *Adv. Mater.* **2012**, *24* (37), 5111-5116.
- [3] Fattah, Z.; Loget, G.; Lapeyre, V.; Garrigue, P.; Warakulwit, C.; Limtrakul, J.; Bouffier, L.; Kuhn, A., Straightforward single-step generation of microswimmers by bipolar electrochemistry. *Electrochim. Acta* **2011**, *56* (28), 10562-10566.
- [4] Castro, C.; Pinault, M.; Coste-Leconte, S.; Porterat, D.; Bendiab, N.; Reynaud, C.; Mayne-L'Hermite, M., Dynamics of catalyst particle formation and multiwalled carbon nanotube growth in aerosol-assisted catalytic chemical vapor deposition. *Carbon* **2010**, *48* (13), 3807-3816.
- [5] Le Goff, A.; Artero, V.; Jusselme, B.; Tran, P. D.; Guillet, N.; Metaye, R.; Fihri, A.; Palacin, S.; Fontecave, M., From Hydrogenases to noble metal-free catalytic nanomaterials for H₂ production and uptake. *Science* **2009**, *326* (5958), 1384-1387.
- [6] Quinson, J.; Hidalgo, R.; Ash, P. A.; Dillon, F.; Grobert, N.; Vincent, K. A., Comparison of carbon materials as electrodes for enzyme electrocatalysis: hydrogenase as a case study. *Faraday Discuss.* **2014**, *172*, 473-496.
- [7] Chen, Y. G.; Wang, J. J.; Liu, H.; Banis, M. N.; Li, R. Y.; Sun, X. L.; Sham, T. K.; Ye, S. Y.; Knights, S., Nitrogen doping effects on carbon nanotubes and the origin of the enhanced electrocatalytic activity of supported Pt for proton-exchange membrane fuel cells. *J. Phys. Chem. C* **2011**, *115* (9), 3769-3776.

- [8] Banerjee, S.; Hemraj-Benny, T.; Wong, S. S., Covalent surface chemistry of single-walled carbon nanotubes. *Adv. Mater.* **2005**, *17* (1), 17-29.
- [9] Peng, Q.; Qu, L. T.; Dai, L. M.; Park, K.; Vaia, R. A., Asymmetrically charged carbon nanotubes by controlled functionalization. *ACS Nano* **2008**, *2* (9), 1833-1840.
- [10] Chopra, N.; Majumder, M.; Hinds, B. J., Bifunctional carbon nanotubes by sidewall protection. *Adv. Funct. Mater.* **2005**, *15* (5), 858-864.
- [11] Qu, L. T.; Dai, L. M., Polymer-masking for controlled functionalization of carbon nanotubes. *Chem. Commun.* **2007**, (37), 3859-3861.
- [12] Lee, K. M.; Li, L. C.; Dai, L. M., Asymmetric end-functionalization of multiwalled carbon nanotubes. *J. Am. Chem. Soc.* **2005**, *127* (12), 4122-4123.
- [13] Wei, Z.; Kondratenko, M.; Dao, L. H.; Perepichka, D. F., Rectifying diodes from asymmetrically functionalized single-wall carbon nanotubes. *J. Am. Chem. Soc.* **2006**, *128* (10), 3134-3135.
- [14] Qu, L. T.; Dai, L. M.; Osawa, E., Shape/size-control led syntheses of metal nanoparticles for site-selective modification of carbon nanotubes. *J. Am. Chem. Soc.* **2006**, *128* (16), 5523-5532.
- [15] Chakrabarti, S.; Gong, K. P.; Dai, L. M., Structural evaluation along the nanotube length for super-long vertically aligned double-walled carbon nanotube arrays. *J. Phys. Chem. C* **2008**, *112* (22), 8136-8139.
- [16] Pint, C. L.; Sun, Z. Z.; Moghazy, S.; Xu, Y. Q.; Tour, J. M.; Hauge, R. H., Supergrowth of nitrogen-doped single-walled carbon nanotube arrays: Active species, dopant characterization, and doped/undoped heterojunctions. *ACS Nano* **2011**, *5* (9), 6925-6934.
- [17] Ma, X. C.; Wang, E. G., CN_x/carbon nanotube junctions synthesized by microwave chemical vapor deposition. *Appl. Phys. Lett.* **2001**, *78* (7), 978-980.

- [18] Koos, A. A.; Dillon, F.; Obraztsova, E. A.; Crossley, A.; Grobert, N., Comparison of structural changes in nitrogen and boron-doped multiwalled carbon nanotubes. *Carbon* **2010**, *48* (11), 3033-3041.
- [19] Koos, A. A.; Nicholls, R. J.; Dillon, F.; Kertesz, K.; Biro, L. P.; Crossley, A.; Grobert, N., Tailoring gas sensing properties of multiwalled carbon nanotubes by in situ modification with Si, P, and N. *Carbon* **2012**, *50* (8), 2816-2823.
- [20] Koos, A. A.; Dowling, M.; Jurkschat, K.; Crossley, A.; Grobert, N., Effect of the experimental parameters on the structure of nitrogen-doped carbon nanotubes produced by aerosol chemical vapour deposition. *Carbon* **2009**, *47* (1), 30-37.
- [21] Hu, P.; Xiao, K.; Liu, Y. Q.; Yu, G.; Wang, X. B.; Fu, L.; Cui, G. L.; Zhu, D. B., Multiwall nanotubes with intramolecular junctions (CN_x/C): Preparation, rectification, logic gates, and application. *Appl. Phys. Lett.* **2004**, *84* (24), 4932-4934.
- [22] Zhang, W. J.; Zhang, Q. F.; Chai, Y.; Shen, X.; Wu, J. L., Gate voltage dependent characteristics of p-n diodes and bipolar transistors based on multiwall CN_x/carbon nanotube intramolecular junctions. *Nanotechnol.* **2007**, *18* (39).
- [23] Wei, D. C.; Liu, Y. Q.; Cao, L. C.; Fu, L.; Li, X. L.; Wang, Y.; Yu, G.; Zhu, D. B., A new method to synthesize complicated multibranched carbon nanotubes with controlled architecture and composition. *Nano Lett.* **2006**, *6* (2), 186-192.
- [24] Sun, S. H.; Jaouen, F.; Dodelet, J. P., Controlled growth of Pt nanowires on carbon nanospheres and their enhanced performance as electrocatalysts in PEM fuel cells. *Adv. Mater.* **2008**, *20* (20), 3900-+.
- [25] Sun, S.; Yang, D.; Zhang, G.; Sacher, E.; Dodelet, J. P., Synthesis and characterization of platinum nanowire-carbon nanotube heterostructures. *Chem. Mater.* **2007**, *19* (26), 6376-6378.

- [26] Sun, S. H.; Zhang, G. X.; Zhong, Y.; Liu, H.; Li, R. Y.; Zhou, X. R.; Sun, X. L., Ultrathin single crystal Pt nanowires grown on N-doped carbon nanotubes. *Chem. Commun.* **2009**, (45), 7048-7050.
- [27] Smith, B. W.; Luzzi, D. E., Electron irradiation effects in single wall carbon nanotubes. *J. Appl. Phys.* **2001**, 90 (7), 3509-3515.
- [28] Chai, Y.; Zhang, Q. F.; Wu, J. L., A simple way to CN_x/carbon nanotube intramolecular junctions and branches. *Carbon* **2006**, 44 (4), 687-691.
- [29] Goswami, G. K.; Nandan, R.; Nanda, K. K., Growth of branched carbon nanotubes with doped/undoped intratubular junctions by one-step co-pyrolysis. *Carbon* **2013**, 56, 97-102.
- [30] Bulusheva, L. G.; Okotrub, A. V.; Fedoseeva, Y. V.; Kurennya, A. G.; Asanov, I. P.; Vilkov, O. Y.; Koos, A. A.; Grobert, N., Controlling pyridinic, pyrrolic, graphitic, and molecular nitrogen in multi-wall carbon nanotubes using precursors with different N/C ratios in aerosol assisted chemical vapor deposition. *Phys. Chem. Chem. Phys.* **2015**, 17 (37), 23741-23747.
- [31] Ago, H.; Ishigami, N.; Yoshihara, N.; Imamoto, K.; Akita, S.; Ikeda, K.; Tsuji, M.; Ikuta, T.; Takahashi, K., Visualization of horizontally-aligned single-walled carbon nanotube growth with ¹³C/¹²C isotopes. *J. Phys. Chem. C* **2008**, 112 (6), 1735-1738.
- [32] Liu, L.; Fan, S. S., Isotope labeling of carbon nanotubes and a formation of ¹²C/¹³C nanotube junctions. *J. Am. Chem. Soc.* **2001**, 123 (46), 11502-11503.
- [33] Khodja, H.; Pinault, M.; Mayne-L'Hermite, M.; Reynaud, C., Carbon nanotube growth mechanism investigated by ion beam analysis. *Nucl. Instrum. Meth. B* **2006**, 249, 523-526.
- [34] Sumpter, B. G.; Meunier, V.; Romo-Herrera, J. M.; Cruz-Silva, E.; Cullen, D. A.; Terrones, H.; Smith, D. J.; Terrones, M., Nitrogen-mediated carbon nanotube growth: Diameter

reduction, metallicity, bundle dispersability, and bamboo-like structure formation. *ACS Nano* **2007**, *1* (4), 369-375.

[35] Tessonnier, J. P.; Su, D. S., Recent progress on the growth mechanism of carbon nanotubes: A review. *ChemSusChem* **2011**, *4* (7), 824-847.

[36] Wirth, C. T.; Bayer, B. C.; Gamalski, A. D.; Esconjauregui, S.; Weatherup, R. S.; Ducati, C.; Baehtz, C.; Robertson, J.; Hofmann, S., The phase of iron catalyst nanoparticles during carbon nanotube growth. *Chem. Mater.* **2012**, *24* (24), 4633-4640.

[37] Pattinson, S. W.; Ranganathan, V.; Murakami, H. K.; Koziol, K. K. K.; Windle, A. H., Nitrogen-induced catalyst restructuring for epitaxial growth of multiwalled carbon nanotubes. *ACS Nano* **2012**, *6* (9), 7723-7730.

[38] Pattinson, S. W.; Diaz, R. E.; Stelmashenko, N. A.; Windle, A. H.; Ducati, C.; Stach, E. A.; Koziol, K. K. K., In situ observation of the effect of nitrogen on carbon nanotube synthesis. *Chem. Mater.* **2013**, *25* (15), 2921-2923.

[39] Boncel, S.; Pattinson, S. W.; Geiser, V.; Shaffer, M. S. P.; Koziol, K. K. K., En route to controlled catalytic CVD synthesis of densely packed and vertically aligned nitrogen-doped carbon nanotube arrays. *Beilstein J. Nanotechnol.* **2014**, *5*, 219-233.

[40] Shao, Y. Y.; Sui, J. H.; Yin, G. P.; Gao, Y. Z., Nitrogen-doped carbon nanostructures and their composites as catalytic materials for proton exchange membrane fuel cell. *Appl. Catal. B* **2008**, *79* (1-2), 89-99.

[41] Quinn, B. M.; Dekker, C.; Lemay, S. G., Electrodeposition of noble metal nanoparticles on carbon nanotubes. *J. Am. Chem. Soc.* **2005**, *127* (17), 6146-6147.

- [42] Sun, C. L.; Chen, L. C.; Su, M. C.; Hong, L. S.; Chyan, O.; Hsu, C. Y.; Chen, K. H.; Chang, T. F.; Chang, L., Ultrafine platinum nanoparticles uniformly dispersed on arrayed CN_x nanotubes with high electrochemical activity. *Chem. Mater.* **2005**, *17* (14), 3749-3753.
- [43] Lin, Y. G.; Hsu, Y. K.; Wu, C. T.; Chen, S. Y.; Chen, K. H.; Chen, L. C., Effects of nitrogen-doping on the microstructure, bonding and electrochemical activity of carbon nanotubes. *Diam. Relat. Mater.* **2009**, *18* (2-3), 433-437.
- [44] Chen, Y. G.; Wang, J. J.; Liu, H.; Li, R. Y.; Sun, X. L.; Ye, S. Y.; Knights, S., Enhanced stability of Pt electrocatalysts by nitrogen doping in CNTs for PEM fuel cells. *Electrochem. Commun.* **2009**, *11* (10), 2071-2076.